Chemical Physics Letters 552 (2012) 92–96

Contents lists available at SciVerse ScienceDirect

Chemical Physics Letters

journal homepage: www.elsevier.com/locate/cplett

Determination of the chiral indices of tungsten disulfide (WS_2) nanotubes by electron diffraction

Hakan Deniz [1], Lu-Chang Qin *

Department of Physics and Astronomy, University of North Carolina at Chapel Hill, Chapel Hill, NC 27599-3255, USA

ARTICLE INFO

Article history:
Received 19 July 2012
In final form 20 September 2012
Available online 27 September 2012

ABSTRACT

An electron diffraction method is described and applied to analyze the atomic structure of individual tungsten disulfide (WS_2) nanotubes. The method is based on a recently developed zoning scheme to determine the chiral indices of nanotubes by nano-beam electron diffraction. The chiral indices of a WS_2 nanotube, which has its outermost shell missing on one end due to uneven growth of shells, is given to illustrate the indexing procedure. We also observed that the tubule chiralities within each WS_2 nanotube display a mono-helical structure on average with a dispersion of a few degrees.

1. Introduction

The successful synthesis of tungsten disulfide (WS_2) nanotubes by Tenne et al. in 1992 proved that formation of tubular nanostructures is not unique to carbon [1]. This was followed by reports of other new types of nanotubes, such as MoS_2, WSe_2, $MoSe_2$, BN, and GaN, in inorganic compounds with layered structures [2–5]. Other examples of metal disulfide nanotubes include TiS_2, ZrS_2, HfS_2, VS_2, NbS_2, TaS_2 and ReS_2 [6–9]. The field of inorganic nanotube research has been growing steadily ever since. The atomic structure of a single shell of metal chalcogenides MX_2 (M = metal; X = S, Se, Te) can be described by a metal layer sandwiched between two chalcogen layers, forming a hexagonal cell. Triple layers are stacked like graphite with only van der Waals interactions between them. The WS_2 layers can be rolled into a cylindrical structure by choosing a specific direction in the two-dimensional (2D) crystal lattice. As for the case of carbon nanotubes (CNTs), this direction can be described by a chiral vector expressed by $\vec{C} = u\vec{a}_1 + v\vec{a}_2$, where $\vec{a}_1$ and $\vec{a}_2$ are the basis vectors of the crystal lattice with an inter-angle of 60° and u and v are two integers which are also named as chiral indices (u,v). The diameter d of a single-shell WS_2 nanotube is given as $d = a\sqrt{u^2 + v^2 + uv}/\pi$, where a = 0.315 nm is the in-plane lattice constant of WS_2 [10].

WS_2 nanotubes exhibit different characteristics from CNTs in terms of their electronic properties. CNTs can be either metallic or semi-conducting depending on their chiral indices, whereas WS_2 (MoS_2) nanotubes are predicted to be semi-conducting regardless of their chirality [11,12]. Recently, this was confirmed by a scanning tunneling microscopy study of WS_2 nanotubes [13]. Synthesis, structure and self-assembly of sub-nanometer single-shell MoS_2 nanotubes of (3, 3) armchair structure have been reported recently with predictions that these tubules might be metallic with a small but finite density of states at the Fermi level [14]. Although bulk WS_2 (MoS_2) nanotubes of armchair structure have a small indirect and moderate direct band gap, it was calculated that zigzag WS_2 (MoS_2) nanotubes will have a small direct band gap whose energy is monotonically increasing as a function of the diameter [11,12]. The report of the synthesis of single- or multi-shell WS_2 nanotubes on template multi-walled carbon nanotubes opens up new possibilities for nano-composite materials and applications, such as solid lubricants, catalysts, scanning probe microscopy tips [15–19]. It is therefore of fundamental importance to have a complete and unambiguous determination of the atomic structure of WS_2 nanotubes in order to understand the structure–property relationships of this nanostructured material.

The structure and defects of WS_2 nanotubes have been studied by high-resolution transmission electron microscopy (HRTEM) and electron diffraction (ED) extensively. Early studies revealed their morphologies where open tips with occasional uneven shells and defective shells were common [20]. Non-chiral nanotubes were mostly armchair type. Thin nanotubes with diameter up to 30 nm were cylindrical whereas thick nanotubes with diameter up to 150 nm had polygonal cross-sections [21]. It was observed that nanotube caps could take rectangular or spherical form depending upon wall thickness and tubule morphology. Nanotubes of mono- and multi-helical structures were identified. Dark-field diffraction contrast imaging showed that mono-helical nanotubes with a dispersion of a few degrees have right-handed chirality [22]. Aberration-corrected HRTEM and Moiré pattern-based techniques combined with structure modeling and image simulations were utilized to obtain the chiral indices of WS_2 nanotubes for better understanding of their growth mechanism [23].

* Corresponding author. Fax: +1 919 962 0480.
E-mail address: lcqin@email.unc.edu (L.-C. Qin).
[1] Present address: Max-Planck Institute of Microstructure Physics, Weinberg 2, 06120 Halle (Saale), Germany.

0009-2614/$ - see front matter © 2012 Elsevier B.V. All rights reserved.
http://dx.doi.org/10.1016/j.cplett.2012.09.041

In this Letter, we present a systematic procedure to identify the atomic structure of a five-shell WS_2 nanotube accurately using electron diffraction and the recently developed zoning scheme. To the best of our knowledge, this is the first time that the chiral indices (u,v) of an inorganic metal disulfide nanotube were determined unambiguously using electron diffraction.

2. Method of analysis

Electron diffraction patterns (EDP) obtained from WS_2 nanotubes resemble very much to those of CNTs in terms of their appearance. Both kinds of nanotubes exhibit layer lines in their diffraction patterns due to the axial periodicity of the tubular structure. Based on the helical diffraction method developed for the determination of the chiral indices of single-walled and multi-walled CNTs, [24–32] we have extended the analytical method to inorganic nanotubes. A major difference of WS_2 nanotubes compared to their carbon counterparts is that they are composed of diatomic molecules. Although the electron scattering intensities of the layer lines from the WS_2 nanotubes are different from the elemental CNTs, their diffraction geometry remains the same. Therefore the well-established nano-beam electron diffraction method can also be used to determine the chirality (chiral indices) of composite nanotubes with a high accuracy.

An electron diffraction pattern of WS_2 nanotube, similar to that of a CNT, consists of two sets of hexagonal spots in reciprocal space such that one set is caused by the top shell and the other by the bottom shell of the nanotube, as schematically illustrated in Figure 1. The finite radial dimension of the nanotube manifests itself as diffraction spots elongated normal to the tubule axis. The diffraction pattern of a multi-shell nanotube is composed of a superposition of the reflections from all shells within the nanotube. For a helical single-shell WS_2 nanotube, there will be two sets of hexagonal reflections appearing as three sets of principal layer lines with respect to the equatorial line in the diffraction pattern. An armchair WS_2 nanotube will exhibit only one layer line which is associated with the $(\bar{1}0)$ reflection while two layer lines associated with (01) and (11) reflections will be observed for a zigzag tubule in the EDP. The spots associated with (02) reflections, which is the manifestation of interference effects due to the stacking of the shells, can also be seen in the EDP for multi-shell nanotubes.

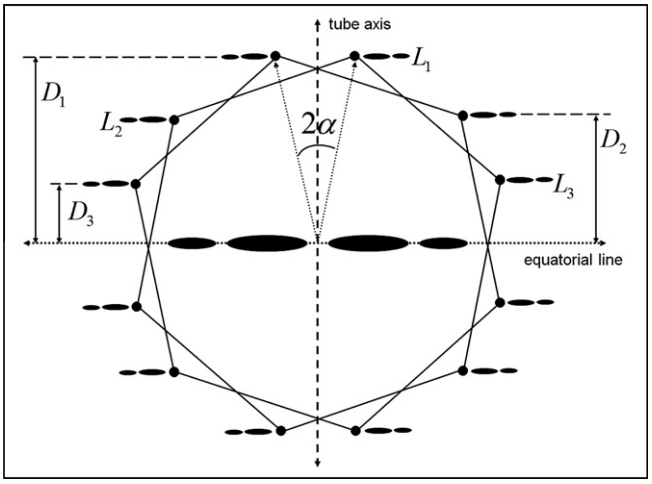

Figure 1. Schematic of electron diffraction pattern of a nanotube formed by a layered structure having a hexagonal lattice. α is the helical angle or helicity of the tubule, L_1, L_2, and L_3 are the principal layer lines and D_1, D_2 and D_3 are the layer line spacings in reciprocal space which are used for calculating the ratio of chiral indices v/u.

When the helicity of each shell of a multi-shell nanotube is different, there will be twice as many hexagonal sets as the number of shells in the diffraction pattern or three times as many principal layer lines on each side of the equatorial line. The first-order reflections of a multi-helicity nanotube can be divided into three zones where each shell with its distinct helicity will have a principal layer line in each of the three zones [32]. These zones are called Z1, Z2 and Z3 zones in reference to the labels of the layer lines in the EDP. The orientation of hexagonal reflections dictates that a zigzag tubule will have a layer line (L1) farthest away from the equator in the Z1 zone and an armchair tubule will have one closest. These two boundaries determine the width of the area (Z1 zone) in which the layer line L1 falls into for all other helicities whose helical angle varies between 0° and 30°. Similarly, the boundaries of other two zones can be determined and the sets of the layer lines corresponding to all helicities can be matched in an orderly fashion [33]. The layer lines L1 and L2 are coincident and the L3 line is located on the equator for an armchair tubule whereas the layer lines L2 and L3 coincide with each other for a zigzag tubule. As the helicity varies from 0° to 30°, the L1 and L2 layer lines move closer to each other and the L3 line moves towards the equatorial line.

To determine the chiral indices (u,v) with a high accuracy, their ratio v/u can be calculated using the measured layer line spacings D_1 and D_2 from the EDP and it can be expressed as[29]

$$\frac{v}{u} = \frac{2D_2 - D_1}{2D_1 - D_2} \tag{1}$$

This equation is not affected by the tilt of the nanotube with respect to the incident electron beam or the camera length at which the EDP was taken [29]. The number of shells and their respective diameter can also be measured from the acquired high-resolution transmission electron microscope (HRTEM) images. In our analysis, the layer line spacings were measured digitally with automated software, which distinguishes and identifies the layer lines from the EDP according to user's specifications, in order to further improve the accuracy. After assigning each layer line into its respective helical set using the zoning scheme, the index ratio v/u and its uncertainty were also calculated. This was followed by finding all possible chiral indices satisfying the measured v/u ratio within the experimental errors and matching the measured diameter closely.

3. Experimental

Transmission electron microscopy and electron diffraction study of WS_2 nanotubes were carried out with JEM-2010F operated at accelerating voltage of 200 kV. The sample was suspended in ethanol by sonication and then transferred onto a lacey carbon coated grid. A nano-probe was generated with the use of the 10 μm condenser aperture by exciting the first condenser lens to maximum to obtain a smallest virtual source. Nano-beam electron diffraction patterns were collected using the parallel beam illumination conditions and recorded on both photographic films and CCD camera at the camera length of 40–60 cm. The diffraction patterns taken on CCD camera were used to measure the intensities on the layer lines since it has a much better dynamical range.

4. Results and discussion

Figure 2a shows a high-resolution TEM image of a five-shell WS_2 nanotube. The outermost shell of this nanotube is not continuous and does not extend to the end of the tubule. Therefore, the nanotube has five shells in one segment and only four shells in the other segment. This is indicated in Figure 2b where the arrows

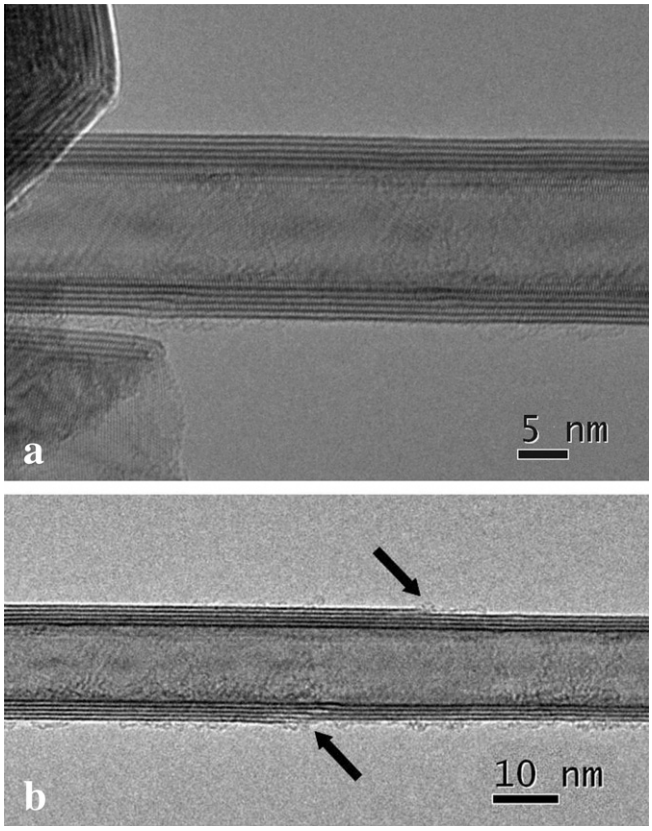

Figure 2. (a) High-resolution TEM image of a five-shell WS_2 nanotube near a fullerene-like WS_2 nanoparticle. (b) High-resolution TEM image of the same nanotube where the outermost layer of the nanotube vanished at locations indicated by arrows.

indicate the positions where the outermost shell ended. Two separate diffraction patterns, taken from the five-shell and four-shell segments, respectively, of this nanotube were obtained on the CCD camera in identical operational settings of the microscope and they are shown in Figure 3a and b, respectively. The diameter of each shell was measured several times from the high-resolution TEM image averaged along the axis of the tubule to reduce the errors due to inconsistencies of measurements. The shell diameters are 16.10, 14.82, 13.61, 12.39, and 11.07 nm in descending order with an uncertainty of ±0.07 nm due to the finite pixel size in the CCD recorded image.

For both electron diffraction patterns, there is only one layer line in the first zone. Five layer lines can be identified in the second and the third zones of the diffraction pattern from the five-shell segment and four layer lines from the four-shell segment. The small separations of the layer lines suggest that this nanotube has a multi-helicity structure with close helicities. The layer lines in the first zone are not resolved from each other due to insufficient resolution of the microscope and that of the recording media. It should also be noted that the width of zone Z1 is also the smallest. Therefore, the layer line spacings D_2 and D_3 were utilized in determining the v/u ratios to minimize the uncertainty. In this case, Eq. (1) is rewritten as

$$\frac{v}{u} = \frac{D_2 - D_3}{D_2 + 2D_3} \tag{2}$$

The error σ_D in the measurement of layer line spacing is used for estimating the error in the v/u ratio through $\sigma_{v/u} = 3\sigma_D\sqrt{D_2^2 + 2D_3^2}/(D_2 + 2D_3)^2$ by error propagation of Eq. (2).

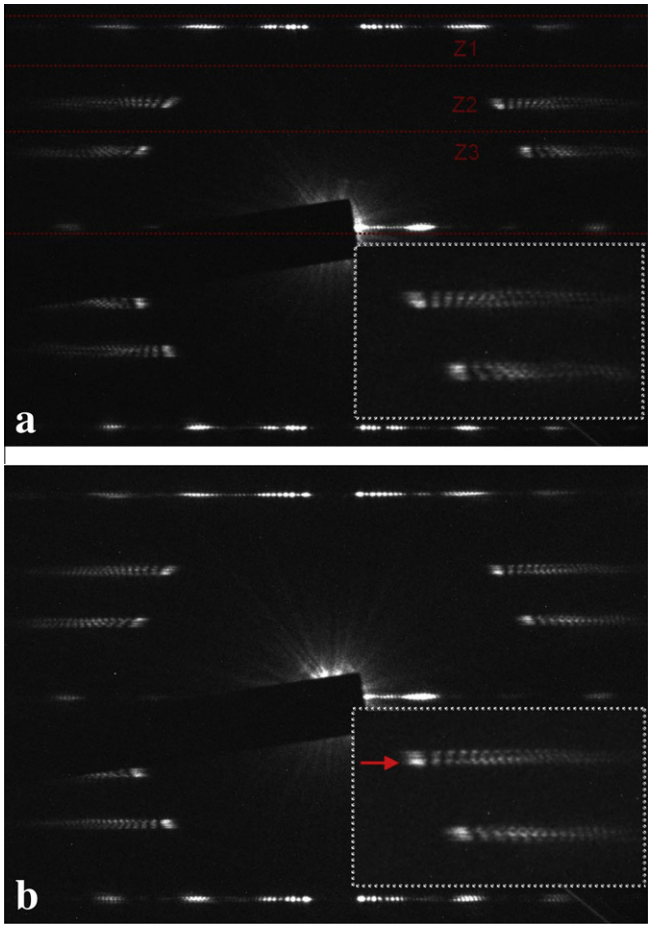

Figure 3. (a) Electron diffraction pattern of the WS_2 nanotube acquired from the five-shell segment of the tubule on CCD camera. Three zones labeled Z1, Z2 and Z3, respectively, are indicated by the dotted red lines in the figure. The inset shows a magnified view of the layer lines where the five layer lines can be distinguished clearly in the Z2 and Z3 zones. (b) Electron diffraction pattern of the same tubule obtained from the part of the tubule with four shells. Again, the inset shows a magnified view of the layer lines (with four lines in Z2 and Z3 zones) where the red arrow points to the layer lines with higher intensity. (For interpretation of the references to colour in this figure legend, the reader is referred to the web version of this article.)

Table 1
Experimentally measured layer line spacings (in arbitrary unit) D_1, D_2 and D_3, uncertainty in layer line spacing σ_D , index ratio v/u, and their propagated errors as percentage for the five-shell WS_2 nanotube shown in Figure 2.

Group	D_1	D_2	D_3	σ_D	v/u	$\sigma_{v/u}$
A	530.9	339.2	189.1	2.6	0.209	2.8
B		335.8	196.0	1.0	0.192	1.1
C		327.5	202.0	1.4	0.172	1.8
D		323.5	208.4	1.0	0.156	1.4
E		319.3	212.0	0.3	0.144	0.5

Table 2
Experimentally measured layer line spacings (in arbitrary unit) D_1, D_2 and D_3, uncertainty in layer line spacing σ_D , index ratio v/u, and their propagated errors as percentage for the four-shell segment of the WS_2 nanotube shown in Figure 2.

Group	D_1	D_2	D_3	σ_D	v/u	$\sigma_{v/u}$
A	529.8	342.4	188.3	1.0	0.214	1.0
B		334.2	192.3	3.3	0.197	3.7
C		327.2	200.4	2.2	0.174	2.7
D		323.7	205.0	1.1	0.162	1.4

Tables 1 and 2 show the measured layer line spacings from each diffraction pattern in arbitrary units and the grouping of the layer lines into their respective helical sets, which was done using the zoning scheme described in the previous section. The tables also list the ratio of the chiral indices v/u for each helicity present. The missing helicity (Group E) from Table 2 is due to the vanishing outermost shell. The layer lines in the second and third zones from both diffraction patterns indicate that groups C, D and E (ranking from lower to higher) should have the highest intensities and group A has the lowest among all (insets in Figure 3a and b). Figure 4 shows a comparison of the intensities of the first peak from the oscillations in the layer lines for each shell. Since the electron scattering amplitude in reciprocal space is proportional to the diameter of nanotube, this means that group E should have the largest diameter and group A the smallest among all shells. This suggests that the best assignment for group A is $(101, 21)$ and for group E is $(151, 21)$ using the measured diameters and the v/u ratios. This also means that the chiral indices of group B, group C, and group D should be $(113, 21)$, $(126, 21)$ and $(139, 21)$, respectively. Table 3 lists the final assignment of chiral indices for this five-shell WS_2 nanotube together with the diameter and helicity of each shell calculated from the assigned chiral indices. A comparison of the measured and calculated v/u ratios with their percent errors is also given in the table.

To improve further the accuracy of the index assignment, we also compared the electron intensity of the equatorial line obtained from the electron diffraction pattern of this nanotube with a simulated intensity calculated using the diameters deduced from the assigned chiral indices as shown in Figure 5. The intensity of the equatorial layer line was calculated using the following equation:

$$I(R) = |F(R, L = 0)|^2 = |f\sum_{i}^{N} d_i J_0(\pi R d_i)|^2 \quad (3)$$

where R is the radial distance from the axis in reciprocal space, f is the atomic scattering amplitude for electrons, d_i is the diameter of the i-th shell, J_0 is the Bessel function of order zero, and N is the total number of shells. Since WS_2 is a binary compound, we used an average atomic scattering amplitude for electrons defined by $f = f_W + 2f_S$ in the simulations. As shown in Figure 5, the assigned chiral indices give rise to a very good agreement of the diffraction peaks.

The nanotubes whose chiral indices have been determined in our Letter manifest a case that the helicity of each shell is only a few degrees apart from one another within a single nanotube. This suggests that the individual shells in the multi-shell WS_2 nanotubes are strongly correlated. The nanotubes that we characterized also tend to have smaller chiral angles toward a zigzag structure (less than 10°). No armchair or zigzag nanotube shells were ever observed in this Letter (see also Table 4). These observations are in agreement with previous findings, [34] but in contrary to the observations of a recent report that a single chiral shell embedded inside non-chiral shells behaves as a template in most cases for the growth of subsequent non-chiral shells within an individual multiwall WS_2 nanotube [23].

The nanotubes studied in our Letter were synthesized in reduction and sulfidization of WO_3 particles with H_2/H_2S gases in a fluidized-bed reactor [35]. Main characteristics of these nanotubes are large hollow cores, open-ended tips and small number of shells on average. This kind of growth mechanism produces mostly helical nanotubes and it was suggested that the helical growth were more favorable both energetically and kinetically because it could help to keep the growth front continuous at the tip of the

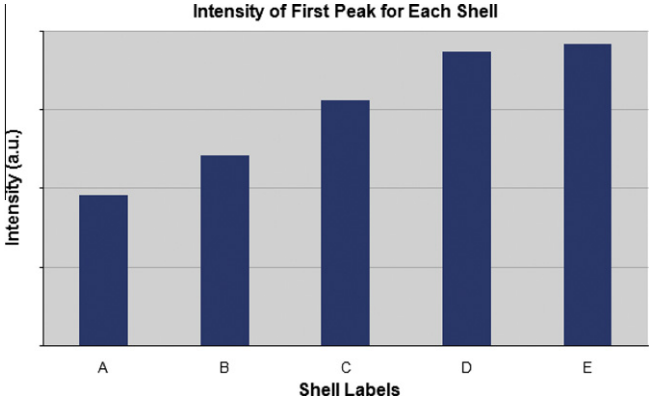

Figure 4. Plot shows the integrated intensity of the first peak obtained from the oscillations in the layer lines L2 of the diffraction pattern shown in Figure 3a for each shell in the WS_2 nanotube.

Table 3
Final assignment of chiral indices (u,v) for the five-shell WS_2 nanotube with an incomplete outer most shell together with the diameters and helicities calculated from the assigned indices. The percent error between the assigned and experimental v/u ratios is also listed.

Group	u	v	d (nm)	v/u	v/u-exp	% error	α (DEG)
A	101	21	11.33	0.208	0.209	−0.7	9.26
B	113	21	12.52	0.186	0.192	−3.2	8.38
C	126	21	13.81	0.167	0.172	−2.8	7.59
D	139	21	15.10	0.151	0.156	−2.9	6.94
E	151	21	16.30	0.139	0.144	−3.7	6.42

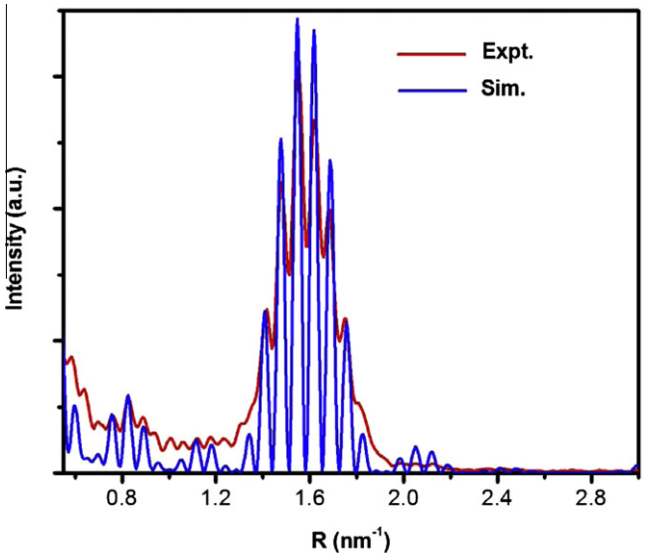

Figure 5. Comparison of experimental intensity (red) of the equatorial layer line and the simulated intensity (blue) using the deduced chiral indices. The intensity profiles are given up to 3 nm^{-1} in reciprocal space to include the (02) reflection. Fine modulations in the simulated curve are in good agreement with the experimental intensity. (For interpretation of the references to colour in this figure legend, the reader is referred to the web version of this article.)

Table 4
Chiral indices (u,v) of three additional WS_2 nanotubes analyzed.

	Chiral indices (u,v)				
WS_2 NT	Shell 1	Shell 2	Shell 3	Shell 4	Shell 5
1	(97,23)	(108,25)	(116,31)	(132,25)	(141,29)
2	(80,19)	(95,15)	(102,22)	(113,22)	(125,22)
3	(90,39)	(98,47)	(112,46)		

nanotube. This is consistent with our observations of the zigzag-like orientation in these nanotubes. For this open-ended growth, we suggest that small variations in the growth rate at the tip were most likely the cause of observed small dispersion in the helicities. Since all shells are growing at the same time, the only way to compensate the changes in growth rate might be a slight change of the helicity in order to provide an even growth of all shells.

The example studied here showed monotonically changing helicities within a nanotube itself where a linear relationship can be drawn between the helicity and diameter whereas no such clear relation was seen for other tubules. This case may suggest that the structure of the nanotube will take the form of achiral type as the diameter increases. Based on this particular nanotube, we estimated that a tubule consisting of 13–14 shells would have an outermost shell with a diameter of about 28 nm with a zigzag structure and exhibit properties completely different than the bulk material. In this way, it might be possible to engineer the nanotube structure precisely for specific applications by controlling synthesis and growth conditions.

The average inter-shell spacing is 0.621 nm, which is only 0.2% larger than the known spacing of WS_2 but it ranged from the smallest of 0.594 nm to the largest of 0.647 nm. A recent study showed that WS_2 is more compressible along the *c*-direction than the *a*-direction [36]. It was also observed the nanoparticle curvature modifies the local charging environment in the intra-shell and inter-shell directions compared to the bulk phase [37]. Such a large variation in inter-shell spacing might be explained by the cumulative effects of the nanotube curvature, sub-oxide contaminants between the shells, compression of the *c*-axis, and occasional structural defects as seen in the HRTEM image given in Figure 2.

Although the shells of the WS_2 nanotube in our Letter have such large diameters, the layer lines in the EDP, especially in the second and third zones, can still be distinguished from one another. The most serious limitation in determining the v/u ratios stems from the overlapping of the first layer line L1 of all shells within the nanotube due to small dispersion of the helicity. The overlapping layer lines can be problematic in general for any two shells with very close helical angles but this error is amplified for the first zone since it has the smallest width. Nonetheless, the electron diffraction method described in this Letter can easily be adapted to determine the chiral indices of other inorganic nanotubes, such as BN and GaN and others cited in the introduction, formed from the layered structures having a hexagonal crystal lattice.

5. Conclusions

The chiral indices of each and every shell of a five-shell WS_2 nanotube have been determined using electron diffraction. The helicities of the shells of this nanotube are different but are close to each other within less than 10°. This distribution of helicity is explained in terms of growth and formation of the nanotube. The experimental technique and method of analysis are generally applicable to all nanotubes with a cylindrical structure.

Acknowledgement

The authors wish to thank Professor R. Tenne for providing the tungsten disulfide nanotube samples used in this Letter.

References

[1] R. Tenne, L. Margulis, M. Genut, G. Hodes, Nature 360 (1992) 444.
[2] Y. Feldman, E. Wasserman, D.J. Srolovitz, R. Tenne, Science 267 (1995) 222.
[3] M. Nath, C.N.R. Rao, Chem. Commun. 21 (2001) 2236.
[4] N.G. Chopra, R.J. Luyken, K. Cherrey, V.H. Crespi, M.L. Cohen, S.G. Louie, A. Zettl, Science 269 (1995) 966.
[5] J.Y. Li, X.L. Chen, Z.Y. Qiao, Y.G. Cao, H.J. Li, Mater. Sci. Lett. 2001 (1987) 20.
[6] M. Nath, C.N.R. Rao, Angew. Chem. Int. Ed. 41 (2002) 3451.
[7] H.A. Therese et al., Angew. Chem. Int. Ed. 44 (2005) 262.
[8] M. Nath, C.N.R. Rao, J. Am. Chem. Soc. 123 (2001) 4841.
[9] M. Brorson, T.W. Hansen, C.J.H. Jacobsen, J. Am. Chem. Soc. 124 (2002) 11582.
[10] W.J. Schutte, J.L. de Boer, F. Jellinek, J. Solid State Chem. 70 (1987) 207.
[11] G. Seifert, H. Terrones, M. Terrones, G. Jungnickel, T. Frauenheim, Solid State Commun. 114 (2000) 245.
[12] G. Seifert, H. Terrones, M. Terrones, G. Jungnickel, T. Frauenheim, Phys. Rev. Lett. 85 (2000) 146.
[13] L. Scheffer, R. Rosentsveig, A. Margolin, R. Popovitz-Biro, G. Seifert, S.R. Cohen, R. Tenne, Phys. Chem. Chem. Phys. 4 (2002) 2095.
[14] M. Remskar et al., Science 292 (2001) 479.
[15] R.L.D. Whitby et al., Chem. Mater. 14 (2002) 2209.
[16] R.L.D. Whitby, W.K. Hsu, C.B. Boothroyd, H.W. Kroto, D.R.M. Walton, Chem. Phys. Lett. 359 (2002) 121.
[17] L. Rapoport, Y. Bilik, Y. Feldman, M. Homyonfer, S.R. Cohen, R. Tenne, Nature 387 (1997) 791.
[18] J. Chen, S.L. Li, Q. Xu, K. Tanaka, Chem. Commun. 16 (2002) 1722.
[19] A. Rothschild, S.R. Cohen, R. Tenne, Appl. Phys. Lett. 75 (1999) 4025.
[20] A. Rothschild, R. Popovitz-Biro, O. Lourie, R. Tenne, J. Phys. Chem. 104 (2000) 8976.
[21] Y.Q. Zhu et al., J. Mater. Chem. 10 (2000) 2570.
[22] L. Margulis, P. Dluzewski, Y. Feldman, R. Tenne, J. Microsc. 181 (1996) 68.
[23] M.B. Sadan, L. Houben, A.N. Enyashin, G. Seifert, R. Tenne, Proc. Nat. Acad. Sci. 105 (2008) 15643.
[24] L.-C. Qin, J. Mater. Res. 9 (1994) 2450.
[25] A.A. Lucas, V. Bruyninckx, Ph. Lambin, Europhys. Lett. 35 (1996) 355.
[26] L.-C. Qin, T. Ichihashi, S. Iijima, Ultramicroscopy 67 (1997) 181.
[27] L.-C. Qin, Chem. Phys. Lett. 297 (1998) 23.
[28] M. Gao, J.M. Zuo, R.D. Twesten, I. Petrov, L.A. Nagahara, R. Zhang, Appl. Phys. Lett. 82 (2003) 2703.
[29] Z. Liu, Q. Zhang, L.-C. Qin, Appl. Phys. Lett. 86 (2006) 191903.
[30] L.-C. Qin, Rep. Prog. Phys. 69 (2006) 2761.
[31] L.-C. Qin, Phys. Chem. Chem. Phys. 9 (2007) 31.
[32] H. Deniz, A. Derbakova, L.-C. Qin, Ultramicroscopy 111 (2010) 66.
[33] H. Deniz, Ph.D. Thesis, University of North Carolina at Chapel Hill, 2007.
[34] R. Rosentsveig, A. Margolin, Y. Feldman, R. Popovitz-Biro, R. Tenne, Appl. Phys. 74 (2002) 367.
[35] A. Margolin, R. Rosentsveig, A. Albu-Yaron, R. Popovitz-Biro, R. Tenne, J. Mater. Chem. 14 (2004) 617.
[36] E. Selvi, M. Yanzhang, R. Aksoy, A. Ertas, A. White, J. Phys. Chem. Sol. 67 (2006) 2183.
[37] R.D. Luttrell, S. Brown, J. Cao, J.L. Musfeldt, R. Rosentsveig, R. Tenne, Phys. Rev. 73 (2006) 035410.